CHEMICAL ENGINEERING TRANSACTIONS
VOL. 100, 2023
A publication of AIDIC
The Italian Association of Chemical Engineering
Online at www.cetjournal.it
Guest Editors: Sauro Pierucci, Flavio Manenti

ISBN 979-12-81206-03-8; **ISSN** 2283-9216
DOI: 10.3303/CET23100052

Numerical Simulation during Development of Taylor–Couette Flow with Shear-thinning Fluids

Hayato Masuda[a]*, Hiroyuki Iyota[a], Naoto Ohmura[b]

[a] Department of Mechanical Engineering, Graduate School of Engineering, Osaka Metropolitan University, 3-3-138 Sugimoto, Sumiyoshi-ku, Osaka, 558-8585, Japan
[b] Department of Chemical Science and Engineering, Graduate School of Engineering, Kobe University, 1-1 Rokkodai, Nada-ku, Kobe, 657-8501, Japan
hayato-masuda@omu.ac.jp

The Taylor–Couette flow between coaxial cylinders with a rotating inner cylinder is a key tool for achieving process intensification. However, this flow system exhibits multistability. For example, the number of Taylor cells formed stochastically depends on the hysteresis and start-up operations in the steady state. To address this issue from a practical perspective, the development process from the start of inner cylinder rotation was investigated using numerical simulations. Two types of fluids, Newtonian and shear-thinning fluids were used. First, it was confirmed that the number of Taylor cells obtained by the simulation agreed with that having the highest probability in the experiments. In addition, the cell size with shear thinning was larger than that of the Newtonian fluid. This is primarily due to the merging of the distorted cell, which is transiently formed, adjoining the end cell. Furthermore, the number of Taylor cells in a steady state with various angular accelerations was tested. Consequently, it was inferred that the number of cells is affected not only by the steady-state time, but also by the function type of the angular acceleration with time.

1. Introduction

Continuous reactors with both excellent mixing performance and narrow residence time distribution (e.g., slug flow reactor (Iwamura et al., 2020) and oscillatory baffled reactor (Avila et al., 2022)) have been attracting attention for achieving process intensification. A Taylor–Couette flow, which is the flow between coaxial cylinders with a rotating inner cylinder, is also suitable for realizing this process intensification. Owing to the toroidal motion in a Taylor cell, mixing and heat/mass transfer are both enhanced. In addition, each cell moves in a single file without causing a breakdown when a relatively small axial flow is introduced. Thus, continuous operation with a narrow residence time distribution is possible. Based on these features, the Taylor–Couette flow has been applied to various chemical processes, such as polymerization (Kataoka et al., 1995), catalytic reactions (Behr and Färber, 2015), and enzymatic reactions (Masuda et al., 2013; Masuda et al., 2017a; Matsumoto et al., 2020).

From a practical perspective, the structure of Taylor cells is one of the most important factors because the cellular structure affects heat and mass transfer performance. According to Ohmura et al. (1998), the axial mass transfer through the boundaries between Taylor cells depends on the vortex height (termed “axial wavelength”), λ, and Reynolds number, *Re*. In particular, they reported that for local mass transfer, the axial wavelength is one of the important parameters. Subsequently, Nemri et al. (2016) summarized the effect of axial wavelength on axial mass transfer using numerical simulations and experiments. Thus, control of the cellular structure is one of the fundamental issues for the application of the Taylor–Couette. This issue is closely related to the multistability of the Taylor–Couette flow, owing to the hysteresis of the flow, determined by the start-up operation. Kataoka (1999) showed that the highest probability of the number of Taylor cells formed in the entire region of the system can be controlled by the angular acceleration of the inner cylinder, α, even though the number of Taylor cells formed is stochastic. In other words, the structure of the Taylor cell is primarily determined by the angular acceleration of the inner cylinder.

Paper Received: 9 January 2023; Revised: 21 April 2023; Accepted: 20 May 2023
Please cite this article as: Masuda H., Iyota H., Ohmura N., 2023, Numerical Simulation During Development of Taylor-couette Flow with Shear-thinning Fluids, Chemical Engineering Transactions, 100, 307-312 DOI:10.3303/CET23100052

To accurately reproduce the flow field of a Taylor–Couette flow, the relationship between the angular acceleration of the inner cylinder and axial wavelength of the Taylor cell must be understood. However, investigations on multistability are limited to Newtonian fluid systems. For chemical engineers, knowledge of non-Newtonian fluids is valuable because most fluids used in the chemical industry exhibit non-Newtonian properties. Nevertheless, the multistability of non-Newtonian fluids (e.g., the effect of start-up operation on the flow state) remains unclear.

Therefore, in this study, the development process of Taylor cells for various *Re* values was simulated using computational fluid dynamics (CFD) to initiate the investigation of the multistability of non-Newtonian fluids. As a non-Newtonian fluid, a shear-thinning fluid was selected owing to its frequent use in chemical industries. In this simulation, a sudden start (i.e., infinite angular acceleration of the cylinder) was conducted. Additionally, five types of acceleration patterns were imposed on a specific case to demonstrate the multi-stability of shear-thinning fluids.

2. Numerical simulation

The computational domain is shown in Figure 1. The radii of the inner and outer cylinders, R_i and R_o, were 0.0125 m and 0.0175 m, respectively. The length of the cylinder, L, was 0.15 m. Geometrical parameters including the gap width, d, radius ratio, ε, and aspect ratio, Γ, are tabulated in Table 1. Considering the boundary condition for the velocity, the velocity at the inner cylinder surface in the circumferential direction was assumed to be $R_i\omega$ (ω is the angular velocity of the inner cylinder). The remaining surfaces were regarded as stationary walls. With respect to pressure, a zero gradient was imposed on all surfaces.

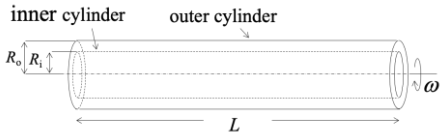

Figure 1: Computational domain

Table 1: Geometrical parameters for the computational domain

R_i [m]	R_o [m]	d (= R_o – R_i) [m]	L [m]	ε (= R_i / R_o) [–]	Γ (= L / d) [–]
0.0125	0.0175	0.005	0.15	0.71	15

The governing equations for the fluid flow are the conservation equations for mass and momentum, given in Eqs. (1) and (2), respectively:

$$\nabla \cdot \mathbf{u} = 0 \tag{1}$$

$$\frac{\partial \mathbf{u}}{\partial t} + (\mathbf{u} \cdot \nabla)\mathbf{u} = -\frac{\nabla P}{\rho} + \frac{1}{\rho}\nabla \cdot (2\eta \mathbf{D}) + \mathbf{g} \tag{2}$$

where **u** is velocity; t is time; P is pressure; ρ is the density; η is the viscosity; **D** is the deformation rate tensor, defined by ($\nabla\mathbf{u} + \nabla\mathbf{u}^T$) / 2; and **g** is the gravitational acceleration.

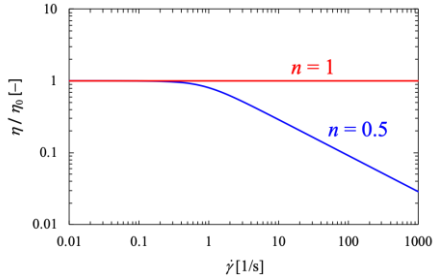

Figure 2: Rheological properties of fluids used in this study

In this study, two types of fluids were used: Newtonian and shear-thinning. The rheological properties of these two fluids are shown in Figure 2. To characterize the rheological properties, the Carreau model (Carreau, 1972) shown in Eq. (3) was used.

$$\eta = \eta_0[1 + (\beta \cdot \dot{\gamma})^2]^{(n-1)/2} \tag{3}$$

where η_0 is the zero shear-rate viscosity; β is the characteristic time; $\dot{\gamma}$ is the shear-rate, defined as $\dot{\gamma} = \sqrt{2\mathbf{D}:\mathbf{D}}$; n is the power-law exponent. The value of β determines the shear-rate at which viscosity begins to decrease. If the value of β is too small, the shear-thinning behavior will not appear. In this study, the value of β was set to 10 s to allow the emergence under a moderate shear-rate flow such as the Taylor–Couette flow. For the value of n, which expresses the degree of viscosity decrease, the condition n = 0.5 was selected as the moderate shear-thinning fluid. It was noted that n = 1 corresponds to a Newtonian fluid.

Owing to the dependence of the viscosity on the shear rate, the definition of Re is complicated in shear-thinning fluids. For practicality, the effective Re, Re_{eff}, is defined using the effective viscosity, η_{eff}, which corresponds to the effective shear-rate, $\dot{\gamma}_{\mathrm{eff}}$. In this study, $\dot{\gamma}_{\mathrm{eff}}$ was calculated using the empirical equation proposed by Masuda et al. (2017b) as follows:

$$\dot{\gamma}_{\mathrm{eff}} = (77.05n^{0.32}\varepsilon^2 - 88.73n^{0.31}\varepsilon + 26.85n^{0.21})\omega \tag{4}$$

The estimated $\dot{\gamma}_{\mathrm{eff}}$ is then substituted to the $\dot{\gamma}$ term in Eq. (3) to obtain η_{eff}. Finally, Re_{eff} was calculated using η_{eff}.

For the simulation, OpenFOAM®4.1 code based on a finite volume method was utilized. The Crank-Nicolson scheme was used for time advancement. A second-order central difference was applied to the viscous and convective terms. The time step was determined by maintaining the Courant number below 0.4. The numerical procedure was identical to that used in previous studies by the authors. The simulation code has been validated in previous studies (Masuda et al., 2017b, Masuda et al., 2019). Therefore, in this section, only the mesh resolution is verified. Figure 3 indicates the mesh system for shear-thinning fluid with the axial distribution of the velocity component in the axial and circumferential directions, u_z and u_θ, along the center line of the gap at Re / Re_{cr} = 2.0 after 2 s from the sudden start of rotation of the inner cylinder for three mesh system types. The number of hexahedral grids 24 × 96 × 72 (system1), 36 × 144 × 108 (system2), and 48 × 192 × 144 (system3) in radial, circumferential, and axial directions, respectively. Noted that Re_{cr} is the critical Re, at which, Taylor vortex flow starts to appear. From the analysis of the linear stability theory by Taylor (1923), Re_{cr} for the geometry in this study (ε = 0.71) is 82.2. As shown in Figure 3, there was no clear difference in the results of system2 and system3. Therefore, to reduce the simulation time, the mesh "system2" was selected.

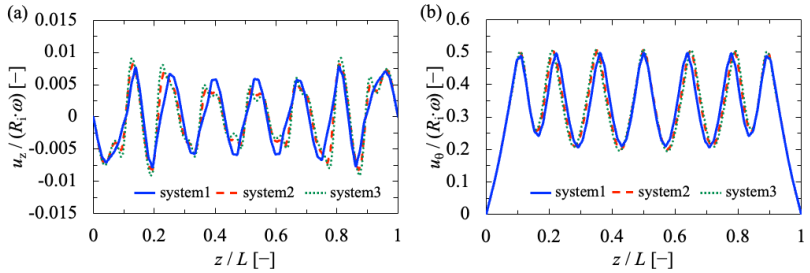

Figure 3: Effect of mesh system on simulation results: (a) circumferential velocity and (b) axial velocity

3. Results and discussion

It is necessary to determine which of the obtained solutions is in a stable state. To date, this issue has not been investigated despite the long history of Taylor–Couette flow problem studies. Thus, the number of Taylor cells formed at steady state, N, was compared between the experimental and simulated results. Data reported by Kataoka (1999) were used to obtain the experimental results. The geometry used in the study by Kataoka (1999), ε = 0.70 and Γ = 22, was different from that used in this study. Therefore, only for this comparison, a geometry of ε = 0.70 and Γ = 22 was used for the simulation. According to Kataoka (1999), at Re / Re_{cr} = 12.0, N = 20 is the highest probability after the sudden rotation of the inner cylinder (i.e., α = ∞ rad/s^2). In the simulation under the same conditions, a value of N = 20 (10 pairs of Taylor cells) was obtained at a steady state. Thus, the highest probability state among the multi-stability states was selected for the numerical simulation as well.

Figure 4 shows the effect of Re / Re_{cr} or (Re_{eff} / Re_{cr}) on the number of cells in the steady state for Newtonian and shear-thinning fluids. For both fluids, the number of Taylor cells decreases with increasing Re / Re_{cr}. This relationship is because the merging of Taylor cells during development was induced by an increase in Re. In addition, at each Re / Re_{cr}, the number of Taylor cells in the shear-thinning fluid was smaller than that in the Newtonian fluid. This tendency indicates that the cell size of the shear-thinning fluid was larger than that of the Newtonian fluid. Although an increase in cell size for shear-thinning fluids has been pointed out by several researchers (e.g., Escudier et al, 1995; Masuda et al., 2019), the detailed mechanism by which it occurs remains unclear. To discuss the cellular structure in more detail, the axial wavelength of the cell, which was normalized by the gap width (d) at each Re / Re_{cr} is shown in Figure 5. Note that the size of "a pair of Taylor cells" instead

of the cell size is shown in Figure 5 (b). It is well known that the end cell, sometimes called the Ekman cell, is larger than the internal cells, owing to the Ekman boundary. For Newtonian and shear-thinning fluids, the sizes of both the cells (end and internal cells) increased with Re / Re_{cr}. In addition, as described above, both sizes (end and internal cells) of the shear-thinning fluid were larger than those of the Newtonian fluid. In particular, the difference in cell size between the Newtonian and shear-thinning fluids was slightly clearer for the end cell than for the internal cells. In other words, in the shear-thinning fluid systems, the increase in the end cell size resulted in a decrease in the number of Taylor cells. Therefore, it can be inferred that shear-thinning affects the development of the end cell and its neighboring cells.

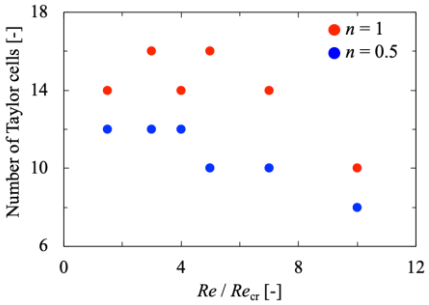

Figure 4: *Effect of Re / Re$_{cr}$ or (Re$_{eff}$ / Re$_{cr}$) on the number of cells at the steady state for Newtonian and shear-thinning fluids*

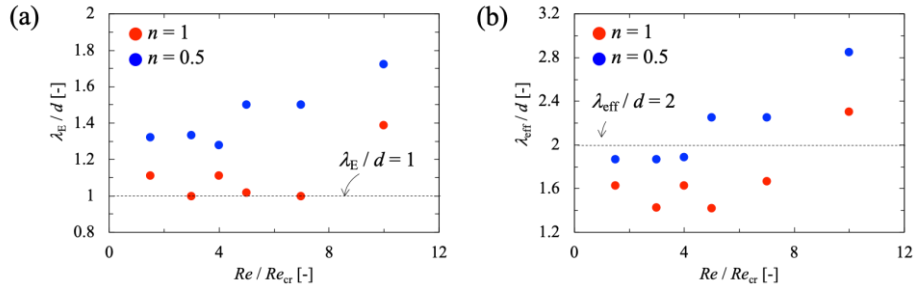

Figure 5: *Effect of Re / Re$_{cr}$ or (Re$_{eff}$ / Re$_{cr}$) on cell size: (a) size of the end cell adjacent to the end wall and (b) averaged axial wavelength of the internal cells*

Figure 6 shows the development process for the velocity vector of the Taylor–Couette flow, focusing on the end cell and neighboring cells at Re / Re_{cr} = 7.0 for (a) Newtonian and (b) shear-thinning fluids. In this figure, the color contours indicate the velocity magnitude distribution for the Newtonian fluid and the viscosity distribution for the shear-thinning fluid. In both systems, the end cell was the first to appear. At the end of the cell development, differences in the development process of the internal cells were observed. In the Newtonian fluid, a small vortex adjacent to the end cell smoothly developed towards the outer cylinder surface. Subsequently, internal vortices developed sequentially. By contrast, the smooth development of the outer cylinder surface was prevented by the viscosity distribution in the radial direction (the viscosity increased along the radius to the outer cylinder surface). In addition, at t = 0.70 s, the axial wavelength of the cell adjoining to the end cell was quite small compared to the gap width, i.e., $\lambda / d << 1$. This distorted cell was unstable, leading to its merging with the end cell. Consequently, a larger end cell was formed. It can be concluded that, in the shear-thinning fluid, merging the transiently formed distorted cell adjacent to the end cell with the original end cell caused an increase in the end cell size, accompanied by larger internal cells compared with the Newtonian fluid system.

Finally, the multistability of the shear-thinning fluid under various startup operations was preliminarily investigated. As shown in Figure 7, the five types of time-dependent angular acceleration of the inner cylinder up to ω = 45.7 rad/s were used: $\alpha_1 = \infty$ rad/s^2, $\alpha_2 = 9.17t$ rad/s^2, $\alpha_3 = 4.57t$ rad/s^2, $\alpha_4 = 0.37t^3$ rad/s^2, and $\alpha_5 = 26.73t^{1/3}$ rad/s^2. After the value of ω reaches 45.7 rad/s^2, the simulation was conducted at a constant ω until t = 20 s. In all cases, ω reached 45.7 rad/s^2 at t = 5 or 10 s. The condition ω = 45.7 rad/s^2 corresponds to Re_{eff} / Re_{cr} = 7.0. The number of Taylor cells at t = 20 s for each angular acceleration is listed in Table 2. As summarized in Table 2, the number of cells N varies widely from 10 to 16, depending on the angular acceleration. In particular, the number of cells for condition α_4 was different from those for conditions α_2 and α_5, despite having the same acceleration time (5s). This result suggests that not only the time for the steady state, but also the type of

function of angular acceleration with time is important. Thus far, the effect of the nonlinear angular acceleration on the number of cells has been investigated. Therefore, in the future, multistability with nonlinear angular acceleration should be investigated in more detail.

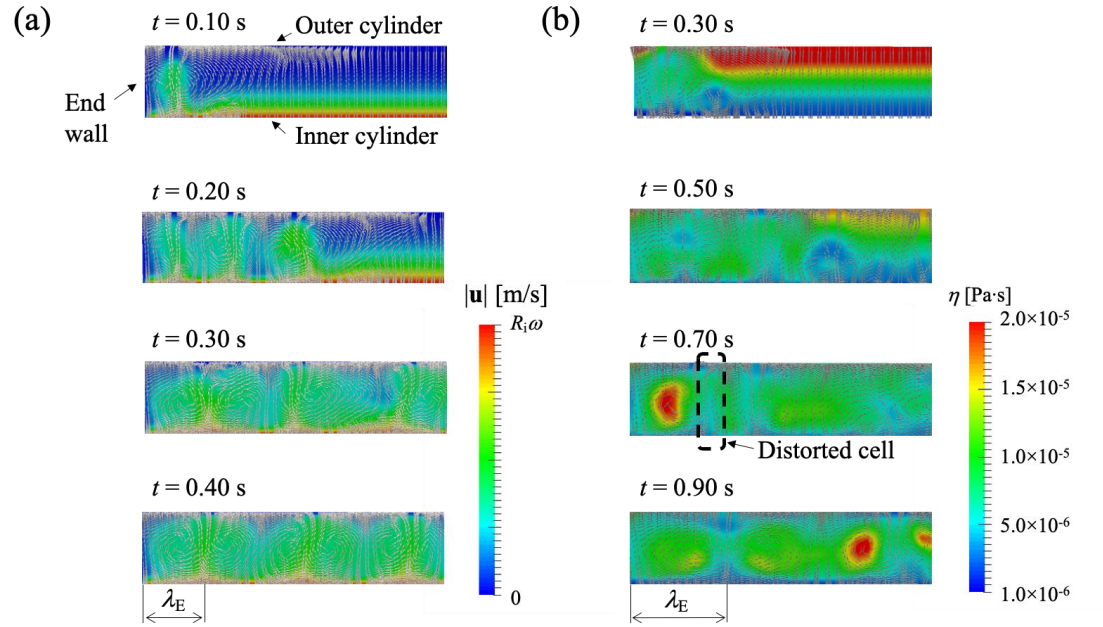

Figure 6 Development process for the velocity vector of Taylor–Couette flow focusing on the end cell and neighboring cells at Re / Re$_{cr}$ = 7.0 for (a) Newtonian and (b) shear-thinning fluids. The color contours show (a) magnitude of velocity and (b) viscosity.

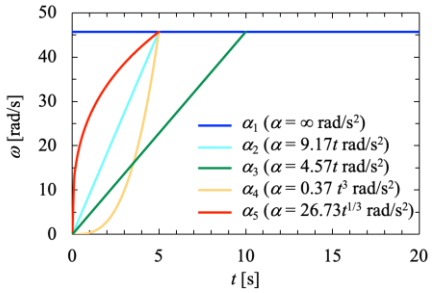

Figure 7 ω with respect to five types of angular acceleration (α)

Table 2: Number of Taylor cells for shear-thinning fluid at steady state with various angular acceleration at Re$_{eff}$ / Re$_{cr}$ = 7.0

	α_1	α_2	α_3	α_4	α_5
N [–]	10	14	12	16	14

4. Conclusions

This study numerically investigated the development process of Taylor–Couette flow with Newtonian and shear-thinning fluids to understand the multistability problem from a practical viewpoint. The following conclusions were deduced:

1. The number of Taylor cells obtained from the numerical simulations agreed with the number from the experiments. Thus, the solution obtained by the numerical simulation corresponds to the selection of the highest probability state in the experiments.
2. The cell size (i.e., axial wavelength) in a shear-thinning fluid system is larger than that in a Newtonian fluid system because of the more complicated development process of Taylor cells. However, in the future, a dependence of rheological parameters on the cell structure should be investigated in more detail.
3. The development with nonlinear angular acceleration showed a wide variation in the number of Taylor cells formed in the annular space. Therefore, more accurate control of the structures of Taylor cells is expected.

Nomenclature

d – gap width, m
D – rate of deformation tensor, 1/s
g – gravitational acceleration. m/s^2
L – cylinder length, m
n – power-law exponent, constant
N – number of Taylor cells, constant
P – pressure, Pa
Re – Reynolds number, constant
Re_{cr} – critical Reynolds number, constant
Re_{eff} – effectiveReynolds number, constant
R_i – inner cylinder radius, m
R_o – outer cylinder radius, m
t – time, s
u – velocity/ m/s
u_z – axial velocity/ m/s
u_θ – circumferential velocity/ m/s
z – axial coordinate, m
α – angular acceleration, rad/s^2
β – characteristic time, s
ε – radius ratio, constant
$\dot{\gamma}$ – shear-rate, 1/s
$\dot{\gamma}_{eff}$– effective shear-rate, 1/s
Γ – aspect ratio, constant
η_{eff} – effective shear-rate viscosity, Pa·s
η_0 – zero shear-rate viscosity, Pa·s
η_∞ – infinite shear-rate viscosity, Pa·s
λ – axial wavelength of Taylor cell, m
λ_E – axial wavelength of end cell, m
λ_{eff} – axial wavelength of internal cell, m
ω – angular velocity, rad/s

Acknowledgments

This research was partially supported by JSPS KAKENHI (Nos. 18H03853, 19KK0127 and 21K14450) from the Japan Society for the Promotion of Science (JSPS).

References

Avila M., Kawas B., Fletcher D. F., Poux M., Xuereb C., Aubin J., 2022, Design, performance characterization and applications of continuous oscillatory baffled reactors, Chemical Engineering and Processing – Process Intensification, 180, 108718.

Behr A., Färber T., 2015, Application of a Taylor-Couette reactor in homogeneous catalysis, Chemical Engineering Transactions, 43, 835–840.

Carrrau P. J., 1972, Rheological equations from molecular network theories, Transactions of the Society of Rheology, 16, 99–127.

Escudier M. P., Gouldson I. W., Jone D. M., 1995, Taylor vortices in Newtonian and shear-thinning liquids, Proceedings of the Royal Society A, 449, 155–176.

Iwamura Y., Horie T., Watabe, Y., Masuda H., Wang S., Hirai K., Kumagai N., Taniya K., Ichihashi Y., Komoda Y., Ohmura N., 2020, Gas absorption enhancement of slug flow in the presence of non-porous silica fine particles, Journal of Chemical Engineering of Japan, 53, 409–413.

Kataoka K., Ohmura N., Kouzu M., Simamura Y., Okubo M., 1995, Emulsion polymerization of styrene in a continuous Taylor vortex flow reactor, Chemical Engineering Science, 50, 1409–1413, 1415–1416.

Kataoka K., 1999, Emergent synthesis of nonlinear phenomena in complex chemical processes and systems, Kagaku Kogaku Ronbunshu, 25, 501–509.

Masuda H., Horie T., Hubacz R., Ohmura N., 2013, Process intensification of continuous starch hydrolysis with a Couette-Taylor flow reactor, Chemical Engineering Research & Design, 91, 2259–2264.

Masuda H., Horie T., Hubacz R., Ohmura N., Shimoyamada M., 2017a, Process development of starch hydrolysis using mixing characteristics of Taylor vortices, Bioscience, Biotechnology, and Biochemistry, 81, 755–761.

Masuda H., Horie T., Hubacz R., Ohta M., Ohmura N., 2017b, Prediction of onset of Taylor-Couette instability for shear-thinning fluids, Rheologica Acta, 56, 73–84.

Masuda H., Shimoyamada M., Ohmura, N., 2019, Heat transfer characteristics of Taylor vortex flow with shear-thinning fluids, International Journal of Heat and Mass Transfer, 130, 274–281.

Matsumoto M., Masuda H., Hubacz R., Horie T., Iyota H., Shimoyamada M., Ohmura N., 2021, Enzymatic starch hydrolysis performance of Taylor-Couette flow reactor with ribbed inner cylinder, Chemical Engineering Science, 231, 116270.

Nemri M., Charton S., Climent E., 2016, Mixing and axial dispersion in Taylor–Couette flows: The effect of the flow regime, Chemical Engineering Science, 139, 109–124.

Ohmura N., Makino T., Motomura A., Shibata Y., Kataoka K., 1998, Intercellular mass transfer in wavy/turbulent Taylor vortex flow, International Journal of Heat and Fluid Flow, 19, 159–166.

Taylor G. I., 1923, Stability of a viscous liquid contained between two rotating cylinders, Philosophical Transactions of the Royal Society, 223, 289–343.